Influence of Initial Pressure on Shock Wave Parameters in Large Explosion Wave Simulation Equipment

Chaoyuan Hang[1,*], Fei Liu[2], Kai Xin[1], Yonghong Gao[1], Yaoyao Zhang[1]

[1]Institute of Defense Engineering, AMS, PLA, Luoyang Henan, 471023, China
[2]Institute of Defense Engineering, AMS, PLA, Beijing, 100850, China

*Corresponding author's e-mail: huangcy725 @163.com

Abstract. In the equipment for simulating explosion waves, the ideal test loading curve can be obtained using high-pressure air drive. To investigate the impact of initial pressure on relevant parameters of shock waves in the test section, AUTODYN16.0 software was employed to simulate the propagation process of shock waves and analyze parameter variations at initial pressures ranging from 100 kPa to 500 kPa. Experimental validation confirms the accuracy of numerical model. The results demonstrate that peak overpressure at the test section outlet ranges from 35 kPa to 111 kPa, with a decrease in energy utilization rate as initial pressure increases. Due to limitations imposed by diaphragm aperture, each parameter's increase amplitude gradually diminishes when initial pressure is raised by increments of 100 kPa; notably, maximum increase amplitudes occur between an initial pressure change from 100 kPa to 200 kPa.

Keywords: High-pressure air; Initial pressure; Shock waves; Numerical model.

1 Introduction

The explosion wave simulation equipment is widely used to replicate the blast wave of conventional and nuclear weapons, typically driven by high-pressure air or explosives. In order to achieve an ideal shock wave loading waveform in the test section, two crucial criteria need to be met: (1) ensuring a stable and smooth shock wave front in the test section; (2) maximizing the positive pressure action time of the shock wave while minimizing charge cooling. To ensure that the generated overpressure-time history curve of the shock wave from this equipment meets practical requirements, it is essential to study and analyze different initial pressures' impact on parameters of the shock wave generated in the test section, thereby determining its variation law and proposing an optimal loading scheme.

Scholars both domestically and internationally have conducted extensive research on the driving technology of explosion wave simulation equipment using various methods, yielding significant progress and outcomes. In terms of numerical simulation, Kiverin A et al. [1] employed fluid mechanics software to conduct a comprehensive numerical investigation into the flow development following shock wave propagation in a tube. The findings indicate that the unstable evolution of the boundary layer within

A. M. Zende et al. (eds.), *Proceedings of the 2024 3rd International Conference on Structural Seismic Resistance, Monitoring and Detection (SSRMD 2024)*, Atlantis Highlights in Engineering 27,
https://doi.org/10.2991/978-94-6463-404-4_6

the shock tube is primarily responsible for variations in the temperature field within it. Thangadurai M et al. [2] utilized a Navier-Stokes solver to examine the interaction between incident shock waves in a shock tube and its structure, elucidating the subsequent development process of tail flow fields post-interaction. Bai Shijie et al. [3] explored how changes in cross-sectional geometry affect flow fields inside a shock tube, summarizing their observations regarding pressure distribution within these tubes when different lengths of contracted cross sections are present. Based on this premise, Zhou Yuelan et al. [4] conducted a study on the high-pressure gas-driven shock tube process and derived the principles governing the impact of shock tube parameters on shock wave characteristics. The findings indicate that adjusting the length ratio between the high-pressure section and low pressure section can enhance the propagation speed of incident and reflected shock waves in space. In terms of experiments, Singh GP et al. [5] utilized a gas-driven shock tube to investigate the impact of varying diaphragm thicknesses on the pressure within the test section. The results demonstrated that an increase in diaphragm thickness led to an elevation in peak differential pressure within the driving section. Herzler J et al. [6] examined the effect of different fuel components on shock wave arrival time under high pressure conditions using a high-energy fuel propulsion method in a shock tube. Tereza Am et al. [7] explored the dynamic mechanism of propane-air mixtures within a shock tube and identified factors influencing combustible gas propulsion. Chen De et al. [8] employed high-pressure air for generating shock waves in a large cross-sectioned shock tube for loading purposes, thereby elucidating damage and failure mechanisms of masonry walls subjected to various explosion loads. Zhang Kunyu et al. [9] employed the finite element analysis software LS-DYNA to investigate the parameters associated with shock wave generation at the termination of the shock tube. The results demonstrated a direct proportionality between peak overpressure and initial overpressure, as well as an inverse relationship with the expansion angle of the transition section. Tian Rui et al. [10] developed an 80mm diameter shock tube and conducted calibration of shock wave parameters within the test section. Furthermore, Sakthi Balan G et al. [11] presented various applications of diverse shock tubes and methods for generating shock waves, thereby offering valuable insights for relevant research.

In summary, the rapid development of high-end weaponry has led to increased demands for the use of explosive wave simulation equipment in resistance detection. However, most current explosion wave simulation equipment fails to meet the requirements for large-scale resistance detection due to limitations imposed by test section size and insufficient research on how initial pressure in the driving section affects shock wave parameters in the test section of such equipment. This study combines numerical simulation and experimentation to investigate variations in shock wave parameters within the test section of large explosion simulation equipment under different initial pressures, providing valuable insights for the development of relevant explosion simulation technology.

2 The establishment of numerical calculation model

In AUTODYN, three algorithms are available for simulating continuum: Arbitrary Lagrange Euler algorithm, Lagrangian algorithm, and ALE (Arbitrary Lagrange Euler) algorithm. The Euler algorithm and ALE algorithm allow the material medium to flow arbitrarily within the grid, while the Lagrangian algorithm ties the material medium to the grid and moves with it. The main difference between these two algorithms lies in whether or not the spatial grid can be moved. In our numerical model, we employ the Euler algorithm for air domains and explosives, whereas the Lagrangian algorithm is used for pipeline structures. To simulate fluid-structure interaction, an automatic fluid-structure coupling method was employed as shown in Figure 1.

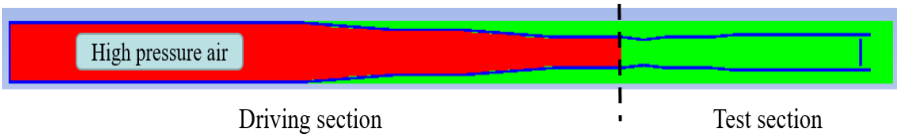

Fig. 1. Numerical calculation model

2.1 Material model

The pipe material steel4340 was selected and described by Johnson Cook strength model. The strength equation of the material is expressed as follows:

$$\sigma = \left[A + B\varepsilon_p^n\right]\left[1 + bC\ln\varepsilon_p^*\right]\left[1 - T^m\right] \tag{1}$$

Where σ is the yield stress, ε is the equivalent plastic strain, T is the temperature, p is the pressure, A is the initial yield stress, B is the hardening constant, C is the strain rate constant, m is the heat softening index, n is the hardening index, and the specific parameter values are as follows: A is 0.792GPa, B is 0.51GPa, C is 0.014, n is 0.26, m is 1.03, the melting temperature is 1793K, and the strain rate correction coefficient is 1.

The TNT charge model is filled in the air domain. Air is described by the ideal gas equation of state, in the following form:

$$p = (\gamma - 1)\rho E \tag{2}$$

The initial air pressure is represented by p, the adiabatic index of air is denoted as γ, the density of air is indicated by ρ, and the specific internal energy of air is represented by E. The values for these parameters can be found in Table 1.

Table 1. Air material parameter

p/(Pa)	ρ/(kg·m-3)	E/(KJ/kg)	γ
1225	1225	206.8	1.4

TNT is described by JWL equation of state in the following form:

$$p_1 = A_1\left(1-\frac{\omega}{R_1V}\right)e^{-R_1V} + B_1\left(1-\frac{\omega}{R_2V}\right)e^{-R_2V} + \frac{\omega E}{V} \tag{3}$$

In the formula, p1 is the detonation pressure, V is the relative volume, E is the initial specific internal energy, A1, B1, R1, R2 and ω are all constants, which are measured by the cylinder experiment. In addition, C-J pressure and energy need to be input, and the values of parameters of TNT material are shown in Table 2.

Table 2. TNT material parameters

ρ/(kg·m^{-3})	A/(GPa)	B/(GPa)	R_1	R_2	ω	V_{CJ}/(m/s)	e/(GJ/m^3)	P_{CJ}/(GPa)
1630	373	3.74	4.15	0.9	0.35	6930	3.68	21

2.2 Calculated working condition

In the numerical simulation of high-pressure air drive, the following reasonable simplifications and assumptions are adopted: (1) Each component gas is considered as an ideal compressible flow; (2) Heat transfer is neglected on the smooth wall surface, thereby disregarding the influence of constrained body walls on the simulation results; (3) The flow field in the main container remains static during the initial stage.

Starting from the safety and applicability of the actual test, the numerical simulation of five operating conditions with initial pressure of 100kPa-500kPa in the driving section was carried out to explore the influence of different initial pressures on related parameters of the shock wave in the test section. The calculation conditions are shown in Table 3.

Table 3. Calculation condition of high-pressure air drive

Working condition	Initial pressure(kPa)
1	100
2	200
3	300
4	400
5	500

2.3 Result analysis

FIG. 2 shows the cloud image of shock wave pressure under different initial pressures when the diaphragm is opened for 500ms. At this time, the maximum pressure corresponding to the initial pressure of 100-500kPa is 23kPa, 82kPa, 141kPa, 201kPa and 262kPa, respectively. It can be seen that the maximum pressure rise amplitude in the response pipeline basically remains unchanged every time the initial pressure increases by 100kPa. And with the increase of initial pressure, the shock wave overpressure in the test section also increases gradually.

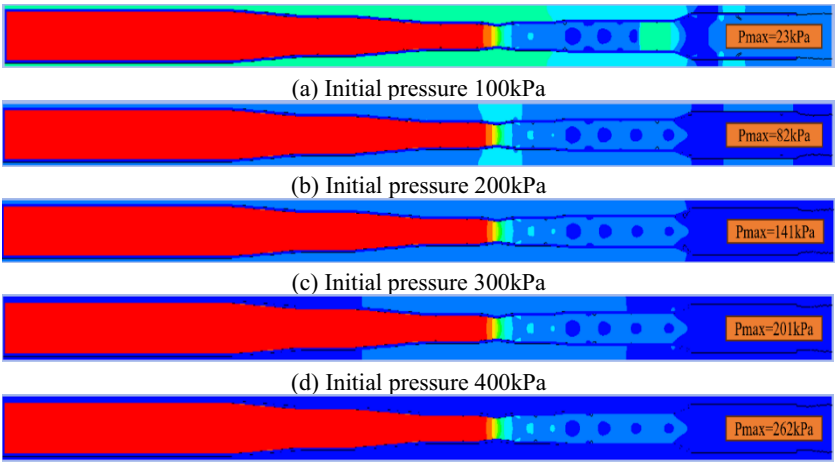

(a) Initial pressure 100kPa

(b) Initial pressure 200kPa

(c) Initial pressure 300kPa

(d) Initial pressure 400kPa

(e) Initial pressure 500kPa

Fig. 2. Pressure cloud image at different initial pressures at the same time

FIG. 3 shows the change process of relevant parameters of incident shock wave at 70m of the test section under different initial pressures. Due to the influence of diffusion at the pipe entrance, the viscosity attenuation of shock wave during its formation and the distance attenuation caused by the development of boundary layer, the intensity of right-moving shock wave gradually weakens. With the increase of initial pressure, the larger the peak value of shock wave overpressure, the longer the duration of positive pressure, and the larger the impulse. In terms of the overall trend, the higher the initial pressure, the greater the value of the relevant parameters of the incident shock wave in the test section, but the growth rate of each parameter decreased significantly, and the decline was the largest when the initial pressure was 100kPa, and the subsequent growth rate tended to be stable. When the initial pressure peak is between 100-500kPa, the peak overpressure at 70 meters of the test section is between 35-111kPa, and the corresponding energy utilization rate is between 22.5% and 35%, which decreases with the increase of the initial pressure. In the test section, the increase amplitude of the peak overpressure of the shock wave per 100kPa is 74.2%, 34.4%, 19.5% and 13.2%, respectively; the increase amplitude of the positive pressure duration is 74.4%, 2.3%, 4.7% and 4.3%; the increase amplitude of the positive pressure impulse is 64.9%, 25.1%, 19.7% and 15.3%. The reason for this phenomenon is due to the limitation of the diaphragm aperture. When the diaphragm aperture is fixed, the greater the initial pressure, the easier the energy is to converge at the diaphragm, forming the phenomenon of shock wave congestion and causing the rise rate of related parameters of the shock wave to decrease.

$$y = 159.17 - 157.37e^{-\frac{x}{422.47}} \tag{4}$$

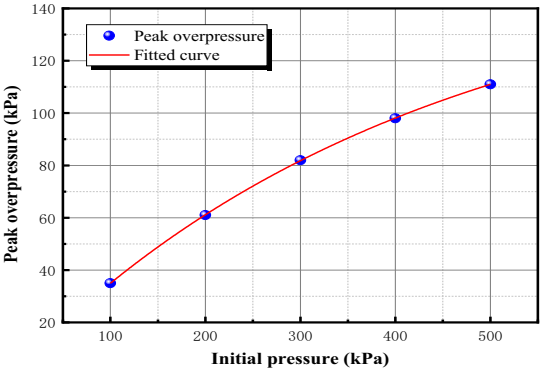

(a) Overpressure peak

$$y = -7709.51e^{(-x/31.34)} - 7709.51e^{(-x/34.83)} - 7709.51e^{(-x/38.31)} + 2680.01 \quad (5)$$

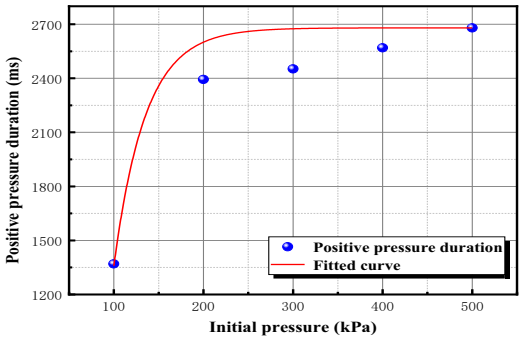

(b) Positive pressure duration

$$y=14834.23+79.51x \quad (6)$$

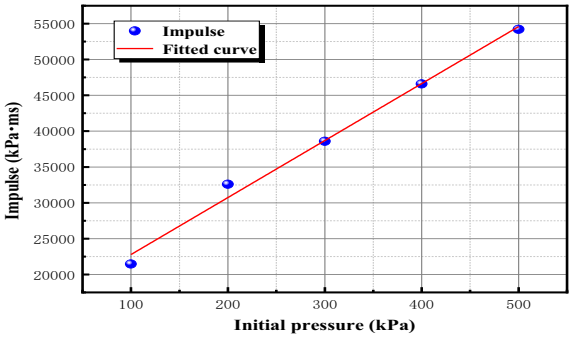

(c) Impulse

Fig. 3. The fitting curve of shock wave correlation parameters at the tail of the test section

3 Test verification

3.1 Test system

The test employed a large-scale explosion wave simulation apparatus, with the driving section having a total volume of approximately 500m3. Furthermore, it was equipped with a high-power inflation device capable of swiftly achieving initial pressure loading ranging from 0 to 500kPa. The diaphragm, made of 5mm thick aluminum, ensured complete incision capability. Refer to Figure 4 for an illustration of the drive segment.

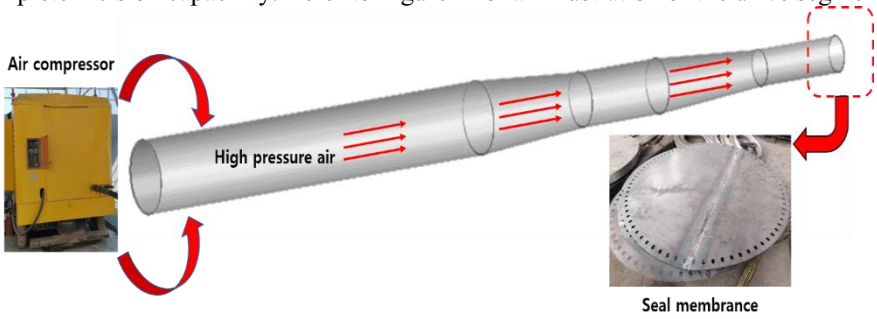

Fig. 4. High pressure air drive section

3.2 Measuring system

The DH5960 super dynamic signal test and analysis system is utilized for data acquisition, featuring a built-in hard disk, transient sampling frequency of up to 10MHz, as well as functionalities like external trigger and signal trigger. Low-noise signal cables are employed for transmitting pressure signals at each test point. The sensor employed is a high-frequency pressure sensor. The configuration of the test system can be seen in Figure 5.

Fig. 5. Test system

3.3 Comparative analysis of results

FIG. 6 shows the comparison curves of overpressure-time-history test and numerical simulation at different measuring points in the test section when the initial pressure is 200kPa. As can be seen from the figure, the shock wave oscillation is relatively serious due to the constraint of pipe wall and the influence of pipe vibration, but it does not affect the interpretation of the peak value of shock wave overpressure and the duration

of positive pressure. On the whole, a high overpressure peak occurs first after the diaphragm is opened, but the positive pressure duration is short. With the increase of distance, the degree of shock wave suture also increases gradually, and the maximum peak positive pressure duration increases obviously. The development trend of the overpressure time history of the numerical simulation results is consistent with that of the test results. With the combined effect of the outflow of high pressure air and the constraint of the pipe wall, the same rapid pressure increase occurs. The pressure increase rate of the numerical simulation is about 18kPa/ms, which is larger than that of the test, because the heat exchange with the outside world is ignored in the numerical simulation process. Table 4 shows the comparison results of shock wave overpressure peak value, positive pressure duration and impulse at different measuring points. From the peak value of overpressure, the difference between the test and the numerical simulation is 8.4%, 6.9% and 6.5%, the positive pressure duration is 9.4%, 16.1% and 6.6%, and the impulse is 9.4%, 5.7% and 5.6%, respectively.

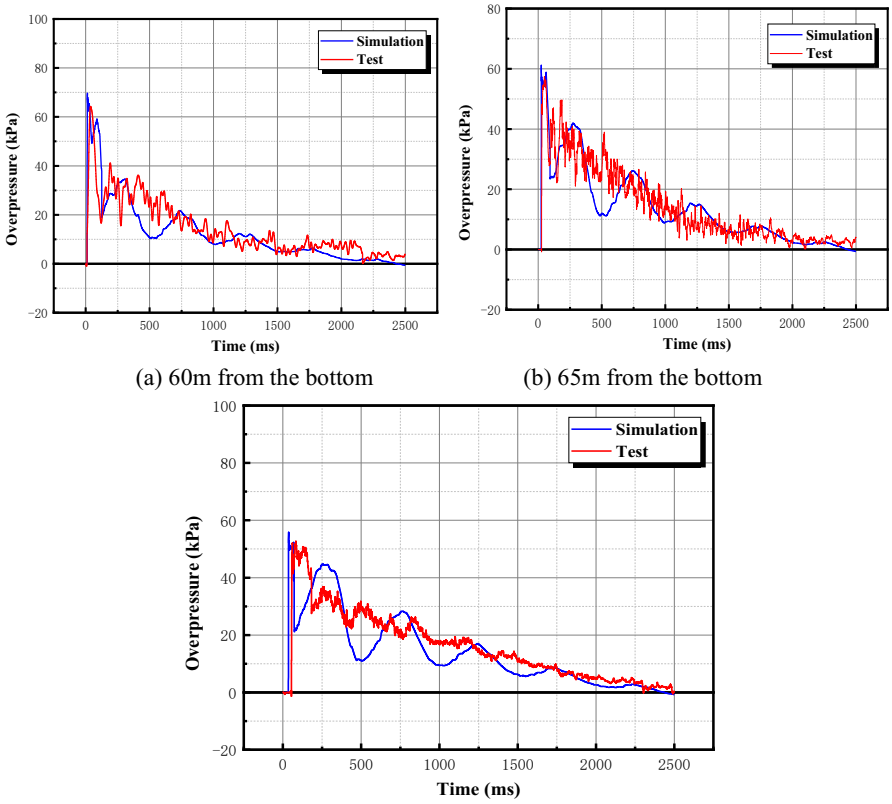

(a) 60m from the bottom (b) 65m from the bottom

(c)70m from the bottom

Fig. 6. Overpressure-time history correlation curve of test point

Table 4. Comparison of shock wave related parameters at different measuring points

Test point	Overpressure peak(kPa)		Positive pressure holding time(ms)		Impulse(kPa·ms)	
	Test	Numeri-cal simu-lation	Test	Numerical simulation	Test	Numerical simulation
T1	64.19	69.61	2167.25	2372.25	33492.66	30338.68
T2	57.22	61.17	2104.04	2441.63	35597.57	33540.97
T3	52.41	55.86	2242.89	2389.63	34585.25	32589.56

In summary, the average relative errors of the peak overpressure, positive pressure duration and impulse are 7.2%, 10.7% and 6.9%, respectively, as shown in Figure 7, and the overall relative error is less than 15%. Therefore, this study believes that the numerical method can simulate the flow field change process in the explosion wave simulation equipment under different driving modes. The reliable and slightly larger shock wave load is also given.

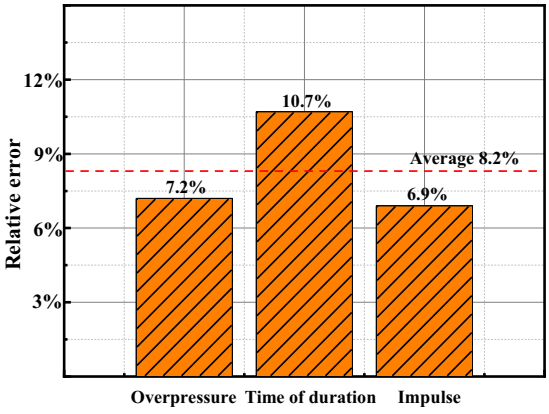

Fig. 7. Average relative error of test and numerical simulation measurement points

4 Conclusion

The AUTODYN16.0 software was utilized in this study to establish a high-pressure gas driving model for simulating large-scale explosion waves. Subsequently, the variation pattern of shock wave-related parameters with respect to the initial pressure in the driving section was analyzed. To validate the accuracy of our numerical calculation model, extensive high-pressure air tests were conducted. Consequently, the following conclusions can be drawn:

(1) With the increase of initial pressure, the larger the peak of shock wave overpressure, the longer the positive pressure duration and the larger the impulse, and the energy utilization rate decreases with the increase of initial pressure. When the high pressure air is driven, the peak value of overpressure at the end of the test section is between

35kPa-111kPa, and the energy utilization rate decreases with the increase of initial pressure.

(2) Due to the limited diaphragm aperture of the equipment, when the initial pressure increases by 100kPa, the increase amplitude of related parameters of the shock wave in the test section gradually decreases, and the increase amplitude of each parameter is the largest when the initial pressure changes from 100kPa to 200kPa.

(3) The relationship between the peak value of overpressure, the duration of positive pressure, the impulse of positive pressure and the initial pressure is fitted with relevant data, and the calculation formula is given. The research results can provide reference for the development of shock wave driving equipment.

References

1. Kiverin A, Yakovenko I (2018) On the mechanism of flow evolution in shock-tube experiments[J]. Physics letters. A, 382(5):309-314. https://doi.org/10.1016/j.physleta. 2017. 11. 033.
2. Thangadurai M, Kundu A and Sandhu I S (2023). Numerical simulation of high peak overpressure blast wave through shock tube and its interaction with a rectangular object[J]. European journal of mechanics, B, Fluids, 97:162-172. https://doi.org/10.1016/j.euromechflu.2022.10.007.
3. Bai S, Liang X and Wang K (2023) Design of Variable Cross Section for Shock Enhancement in Shock Tubes. Journal of Combustion Science and Technology. 29(4):406-413.
4. Zhou Y, Pei L, Long R, Zang Q, Liu B and Ren J (2023) Study on the Evolution Characteristics of Pressure Pulse in Shock Tube and the Method of Simulating Air Explosion Shock Wave[J]. Acta Armamentarii. 2023:1-11.
5. Singh G P, Sharma J D and Arora R (2020). CFD analysis of shock tube for blast impact testing[J]. Materials today: proceedings. 28:1872-1878. https: //doi. org/ 10. 1016/ j.matpr. 2020.05.294.
6. Herzler J, Fikri M and Schulz C. (2020) High-pressure shock-tube study of the ignition and product formation of fuel-rich dimethoxymethane (DMM)/air and CH4/DMM/air mixtures[J]. Combustion and Flame. 216:293-299. https://doi.org/10.1016/j.combustflame. 2020.03.008.
7. Tereza A M, Kozlov P V and Gerasimov G Y. (2023) Shock-tube study of high-temperature ignition of propane-air mixtures at elevated pressures[J]. Acta astronautica, 204:705-710. https://doi.org/10.1016/j.actaastro.2022.11.001.
8. Chen D, Wu H Chen S and Wei J (2023) Shock tube tests and dynamic behavior analyses on one-way masonry-infilled walls. Explosion and Shock Waves. 43(8):134-152.
9. Chen D, Chen D amd Wu H (2023) Mumerical Simulation andParametric Analysis of High-Pressure Gas-Driven Shock Tube. Chinese Journal of High Pressure Physics. 37(3):7-17.
10. Tian R, Wei G, Zhang H, Wu Q and Deng Y 2023 Study of the blast resistance of GFRP laminates based on air shock tube. Composites Science and Engineering. (3):68-75.
11. Sakthi Balan G and Aravind Raj S.(2023) A review on Shock tubes with multitudinous applications[J]. International journal of impact engineering, 172:104406. https: //doi. org/ 10. 1016/j.ijimpeng.2022.104406.